Available online at www.CivileJournal.org

Civil Engineering Journal

(E-ISSN: 2476-3055; ISSN: 2676-6957)

Vol. 10, No. 02, February, 2024

Effect of Different Ceramic Waste Powder on Characteristics of Fly Ash-Based Geopolymer

Bernardinus Herbudiman [1], Subari Subari [2], Bactiar Nugraha [1], Indah Pratiwi [3*], Asnan Rinovian [4], Euneke Widyaningsih [1], Evi Dwi Yanti [4], Bagus D. Erlangga [3, 5], Jakah Jakah [3], Seto Roseno [2]

[1] *Department of Civil Engineering, Institut Teknologi Nasional (ITENAS), Bandung, 40124, Indonesia.*

[2] *Research Center for Advanced Materials, National Research and Innovation Agency (BRIN), Banten, 15314, Indonesia.*

[3] *Research Center for Geological Resources, National Research and Innovation Agency (BRIN), Bandung, 40135, Indonesia.*

[4] *Research Center for Mining Technology, National Research and Innovation Agency (BRIN), Lampung, 35361, Indonesia.*

[5] *Department of Civil, Environmental and Mining Engineering, The University of Western Australia, Perth, 6009, Australia.*

Received 25 October 2023; Revised 19 January 2024; Accepted 23 January 2024; Published 01 February 2024

Abstract

The escalating demand for construction materials driven by rapid population growth has heightened the reliance on cement binders, resulting in increased CO_2 emissions from the cement industry. Geopolymers, considered environmentally friendly alternatives, have been explored in various studies to address this challenge. This research specifically investigates the impact of different types of ceramic waste bricks (BT), floor tiles (FT), roof tiles (RT), and sanitary ceramics (ST) on the physical and mechanical properties of fly ash-based geopolymer mortar. To provide a comprehensive understanding, this research examines the compressive strength, mineral phase, chemical bonds, and microscopic evolution of fly ash geopolymer mortar incorporating varying proportions of each ceramic waste type (25% and 50% fly ash replacement). A consistent mixture of Na_2SiO_3 and NaOH was used for the alkaline solution in all formulations. The curing process was carried out at room temperature for 7, 14, and 28 days prior to the compressive strength test. The result revealed that the inclusion of 25% BT experienced higher strength compared to the control sample after 14 days, but the strength became comparable after 28 days at 40.24 MPa. A reduction in strength was evident with the addition of other ceramic components. Moreover, higher incorporation of CWP correlated with a faster setting time for fresh geopolymers. This was also linked to the degree of gel formation, as indicated in the microstructure images. The emergence of plagioclase minerals was evident in all formulations of the geopolymer products under XRD analysis, while the bond of the geopolymer signature, Si-O-T (T = Si or Al), was identified from the infrared spectra. The microstructure of the binder showed a geopolymer matrix alongside unreacted fly ash particles. Overall, CWP replacement up to 25% can be potential in fly ash geopolymer without sacrificing significant strength loss and remaining in the range of normal strength mortar.

Keywords: Geopolymer; Fly Ash; Ceramic Waste; Precursor; Compressive Strength.

1. Introduction

One of the impacts of rapid population growth is that it can cause an increase in demand for construction and infrastructure. Demand for cement, the primary building material, is also increasing, resulting in increased CO_2 emission pollution due to the burning of fossil fuels in making cement [1]. The cement industry is the second-largest source of

* Corresponding author: inda014@brin.go.id

http://dx.doi.org/10.28991/CEJ-2024-010-02-06

CO_2 emissions after the iron and steel industry [2], making it one of the main sectors causing the greenhouse effect. Around 60% of CO2 emissions are produced by the calcination process of limestone (CaCO3), with the remaining 40% burning coal for heating kilns to produce clinker [3]. Conventional cement production also requires large amounts of raw materials such as limestone, clay, sand, and other additives. The exploitation and transportation of these raw materials cause environmental degradation, including deforestation, soil erosion, and damage to ecosystems [4]. To overcome the negative impact of the cement industry on the environment, it is very important to develop alternative sustainable construction material technologies that are environmentally friendly, such as geopolymers. Geopolymer is a synthetic material formed through a chemical reaction between inorganic materials that are rich in aluminosilicate compounds and alkaline activators [5]. In the process of mixing raw materials with alkaline activators such as sodium or potassium hydroxide, a chemical reaction occurs that forms polymer bonds in the geopolymer matrix. Geopolymers are generally made using raw materials such as fly ash, industrial waste, volcanic ash, or natural soils that are rich in silica and alumina.

Fly ash is a waste produced from burning coal in a power plant that is very fine in size and contains the minerals silica (Si), alumina (Al), iron (Fe), calcium (Ca), and several other minerals. The production of fly ash-based geopolymers helps reduce dependence on conventional cement to reduce CO_2 emissions [6, 7]. Geopolymers made from fly ash have good mechanical and thermal properties, equivalent to or even better than conventional concrete, and are resistant to aggressive environments [7, 8]. However, the strength gain in fly ash-based geopolymers is mostly dependent on heat curing [9]. One of the promising approaches to reaching optimum early strength at ambient temperature was to incorporate GGBS slag, which provides calcium oxide (CaO), into the reaction, promoting hydration products [10]. In terms of high calcium fly ash, the inherent CaO compound can lead to this early strength performance in the geopolymer. Although the mixed reaction relies on the combination of geopolymer and hydration products, this can still be beneficial in ambient curing applications.

Apart from fly ash, waste generated from the ceramics industry can also be used as a raw material in the manufacture of geopolymers. In practice, the physical and mechanical properties of geopolymers are affected by the type of ceramic waste used. The chemical make-up of the ceramic waste could affect the physical and mechanical properties of geopolymers. This has an impact on the reactivity and bond strength (microstructure) that are formed. With a finer and more homogeneous particle size of ceramic waste, the surface area of the material can be increased, and chemical reactions can be accelerated during geopolymer formation [11–15]. The use of ceramic waste in the manufacture of geopolymers can have an impact on the porosity and density of the material being made. The quantity and size of the geopolymer's pores will affect its mechanical properties, such as strength and resistance to cooling. Incorporation of some ceramic waste as an aggregate in geopolymer has shown potential for improving mechanical performance [16], [17]. The quality of the bond formed is also influenced by the way the ceramic waste particles interact with the geopolymer matrix, as indicated by the interfacial transition zone [17]. The geopolymer structure can be damaged if the particle-matrix interaction is weak [18, 19]. However, the application of ceramic waste powder (CWP) as a precursor would be a completely different mechanism.

Rashad et al. 2023 [20] developed a fly ash-based geopolymer by utilizing tile waste as a substitute material for fly ash with a 10–50% percentage. The addition of waste tile powder up to 40% increases compressive strength. Meanwhile, adding 50% tile powder waste has a detrimental effect on compressive strength. This is caused by the presence of an excessive number of fine particles, which inhibit the polymerization reaction and cause pore formation. Similar research revealed that partial replacement of 15% fly ash by ceramic wall tile waste powder in geopolymer concrete provided similar compressive strength, increased split tensile strength by 3%, and increased elastic modulus by 7%. These findings suggest that ceramic waste powder can be used to replace 10–15% of fly ash in M35-grade structural geopolymer concrete, which can be cured under ambient conditions [21]. In addition to tile waste, red clay brick waste can also be used as a precursor to geopolymers. Replacement of 33.3% metakaolin by red clay brick waste in the geopolymer adhesive did not cause a decrease in compressive strength compared to pure metakaolin geopolymer here. Even though it has a lower adhesive phase, mortar with red clay brick waste of 33% and 50% shows the maximum compressive strength value [22]. Sanitaryware has also been researched to become a substitute material for aggregates and geopolymer precursors. Allaoui et al. (2022) [15] investigated the potential for reusing sanitaryware waste as aggregate to produce metakaolin-based geopolymer concrete. The research results show that the developed concrete has higher mechanical performance than conventional concrete and reference geopolymers. It is also proven that increasing the aggregate particle size significantly influences compressive strength, density, and porosity. Other research also investigated geopolymer mortar's mechanical and microstructural characteristics with recycled sanitary ceramic waste powder exposed to high temperatures. The highest strength was obtained in CSW-M prepared with 16 M NaOH and a ratio of 0.45 w/w [23].

Based on previous research exploring the potential of various types of ceramic waste as a substitute for geopolymer precursors, this study aims to compare the effect of various types of ceramics, such as bricks (BR), floor tiles (FT), roof tiles (RT), and sanitary ceramics (ST), as a geopolymer precursor for their physical and mechanical properties. This research seeks to understand and enhance the potential of fly ash-based geopolymers and ceramic waste as sustainable

construction materials. The performance of the resulting geopolymer could be significantly influenced by the characteristics of each ceramic waste. As traditional ceramics comprise various types, it is worth noting that a study on this topic could provide perspectives on further utilizing ceramic waste. The use of these materials in the manufacture of geopolymers can also help reduce the consumption of limited natural resources, minimize industrial waste, and decrease the environmental impact of industrial construction.

2. Material and Methods

2.1. Material

Fly ash (FA) from a coal power plant was utilized as the main precursor in the control mix. The ceramic waste consisted of four types, namely brick (BR), floor tiles (FT), roof tiles (RT), and sanitary ceramics (ST). These ceramic wastes were derived from rejected products in the ceramic production industry. They were initially comminuted using a laboratory mill and then sieved to obtain –75 µm particles of ceramic waste powder (CWP). A local river sand was chosen as the natural fine aggregate for all mixtures. The particle size of the raw materials was measured using a Mastersizer 2000 particle size analyzer. The particle size distribution of precursor materials is depicted in Figure 1. It is evident that all types of CWP exhibit larger particle sizes compared to fly ash. This observation holds particular significance in the field of geopolymers, where particle size plays a critical role in influencing the properties of the resulting materials.

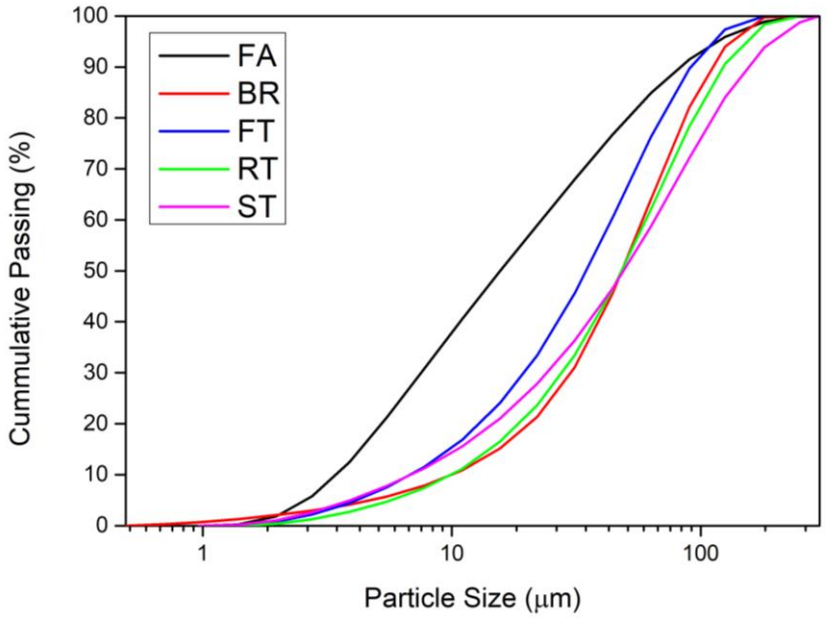

Figure 1. Particle size distribution of precursor materials

The larger particle size of CWP can indeed have a profound impact on various aspects of geopolymer properties. Firstly, particle size affects the reactivity of the precursors during geopolymerization. Smaller particles result in an increased surface area, facilitating a more rapid reaction with the alkaline reagent. This, in turn, can contribute to shorter setting times and higher early strength in the geopolymer. In contrast, larger particles may require more time to fully react, influencing the curing period required for optimal strength development [24, 25]. Secondly, the mixing behavior of these materials can be affected by particle size. Larger particles may lead to challenges in achieving a homogenous mixture, potentially resulting in variations in the geopolymer's properties such as strength, density, and porosity. The distribution of particle sizes in the mixture can also impact the flowability and workability of the geopolymer paste during casting and molding processes [26–28]. With the identical particle size distribution of all CWP, this can enhance the effective comparison for the resulting geopolymer.

Furthermore, Table 1 shows the chemical composition of the precursor materials that were examined using XRF analysis. The FA precursor contained high amounts of CaO and Fe_2O_3, with concentrations of 25.59% and 29.91%, respectively. Based on ASTM C618 [29], this fly ash belongs to class C, with total SiO_2, Al_2O_3, and Fe_2O_3 being within the range of 50%-70% and CaO exceeding 10%. The chemical composition of FA, BR, FT, RT, and ST precursors was dominated by SiO_2, Al_2O_3, and Fe_2O_3 with a quantity of 68.68%, 66.44%, 58.58%, 94.34%, and 87.13%, respectively. RT and ST precursors contained SiO_2 greater than 50% with a quantity of 61.94% and 63.97%, respectively.

Table 1. Chemical composition and physical properties of precursor materials

Oxides, %	FA	BR	FT	RT	ST
SiO_2	27.73	37.36	37.87	61.94	63.97
Al_2O_3	11.03	12.61	10.45	17.58	19.30
Fe_2O_3	29.91	16.47	10.26	14.82	3.86
CaO	25.59	3.57	6.49	0.64	3.78
SO_3	1.73	0.19	0.00	-	-
K_2O	1.59	1.01	2.79	2.16	4.71
TiO_2	1.17	1.55	1.20	1.44	0.63
MnO	0.25	0.36	0.25	0.11	0.05
ZrO_2	0.04	0.06	0.66	0.08	2.15
Density (g/cm^3)	2.50	2.00	2.38	2.08	2.65
Average Particle Size [4, 3] (µm)	32.66	55.14	42.92	58.47	66.25
Specific surface area (m^2/g)	0.68	0.35	0.37	0.27	0.34
D_{10} (µm)	3.48	10.05	6.91	10.01	6.87
D_{50} (µm)	15.8	48.31	34.81	48.19	48.86
D_{90} (µm)	84.53	109.80	91.4	122.66	152.26

The range of mineral phases in the starting materials is shown in Figure 2. The fly ash (FA) component was found to be composed of calcite, quartz, and hematite. In contrast, BT contained solely quartz and anorthite. Interestingly, the other CWP constituents (FT, RT, and ST) exhibited similar mineral phases, including quartz, hematite, and mullite.

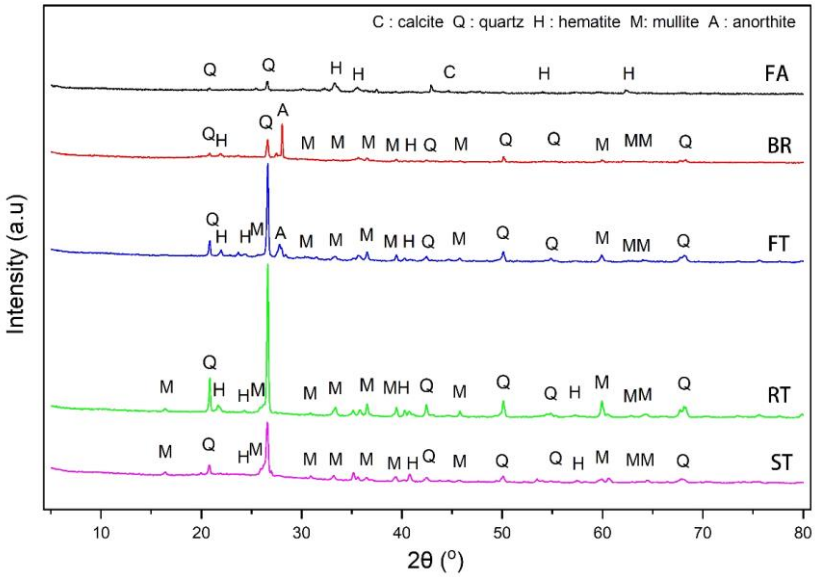

Figure 2. XRD pattern of starting materials

Based on Scanning Electron Microscopy (SEM) analysis, as shown in Figure 4, fly ash particles have a spherical shape, while the four types of ceramic waste present angular particle shapes. The alkaline solution used to produce geopolymer specimens is a mixture of sodium hydroxide solution (NaOH) and sodium silicate/waterglass (Na_2SiO_3) with a ratio of 1:3. Flakes of NaOH of 99% purity were dissolved using distilled water to reach a concentration of 14 M, then cooled for 24 hours prior to the mixing process. Furthermore, the NaOH solution is mixed with Na_2SiO_3 with a grade of 58. Natural river sand passing through sieve no. 4 (-4.76 mm) and being retained on sieve no. 100 (+0.149 mm) was used as fine aggregate, which has a density of 2.42 kg/m^3, fineness modulus at 2.7, and water absorption at 2.46%.

2.2. Preparation, Casting, and Curing of Specimen

The geopolymer mixtures were prepared by combining 70% fine aggregate and 30% binder based on volume percentage. The binder is a mixture of 60% precursor and 40% alkaline solution. Fly ash, as the precursor, was then

substituted by each ceramic waste with a proportion of 25% and 50%. The flow charts for this procedure are illustrated in Figure 3. The proportions of mixed materials needed to produce geopolymer mortar specimens based on weight ratio on the basis of fly ash in GC were presented in Table 2. The solid materials were mixed until homogenized, and subsequently, the sodium silicate and natrium hydroxide solutions were added. The fresh mixture was cast into 50×50×50 mm cubes. After 24 hours, the specimens were removed from the mold and cured at room temperature, covered with a plastic membrane to prevent rapid water evaporation from the specimen. Compressive strengths were performed at the ages of 7, 14, and 28 days.

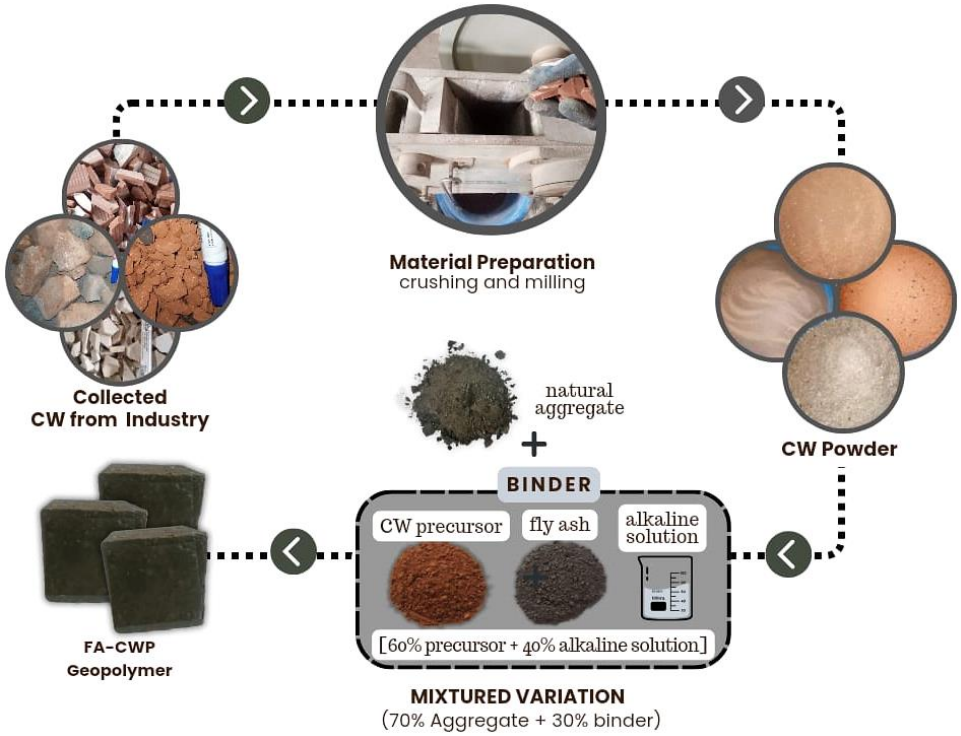

Figure 3. Flow chart of fly ash-CWP geopolymer production

Table 2. Mix proportion of geopolymer specimen (weight ratio in respect to FA in GC)

Mix	Sand	Fly Ash	Ceramic waste type				NaOH (14 M)	Na_2SiO_3
			BR	FT	RT	ST		
GC	3.76	1.00						
G-25 BR	3.76	0.75	0.20					
G-50BR	3.76	0.50	0.40					
G-25 FT	3.76	0.75		0.24				
G-50 FT	3.76	0.50		0.47			0.14	0.48
G-25 RT	3.76	0.75			0.21			
G-50 RT	3.76	0.50			0.42			
G-25 ST	3.76	0.75				0.27		
G-50 ST	3.76	0.50				0.53		

Figure 4 (left) shows the colors of powder samples FA, BR, FT, RT, and ST as brownish black, reddish dark brown, light brown, reddish dark brown, and white, respectively. Iron oxide content is one of the factors that influences the color of ceramic waste powder. BR and RT samples exhibit an intense red color, while FT and ST samples display a lighter color. This is shown by the chemical composition, where the BR sample has the highest hematite content, followed by the RT, FT, and ST samples, where the hematite content is lower. Ceramic waste was ground into powder form. Then, each powder was characterized by its morphology using SEM (Figure 4 right). The SEM image of fly ash (Figure 4-a) clearly shows distinct spherical particles with heterogenous sizes, indicating the varying composition of this material, commonly produced as residue from coal combustion. Meanwhile, the ceramic waste powder sample (Figures 4-b and 4-e) shows an assortment of particles characterized by asymmetrical forms and sharp edges. Of the four types of ceramic waste powder, the roof tile (RT) samples have an average size that is smaller than the others (see Figure 4-d). Meanwhile, the particles from the floor tile (FT) sample exhibit higher density compared to the other samples (see Figure 4-c).

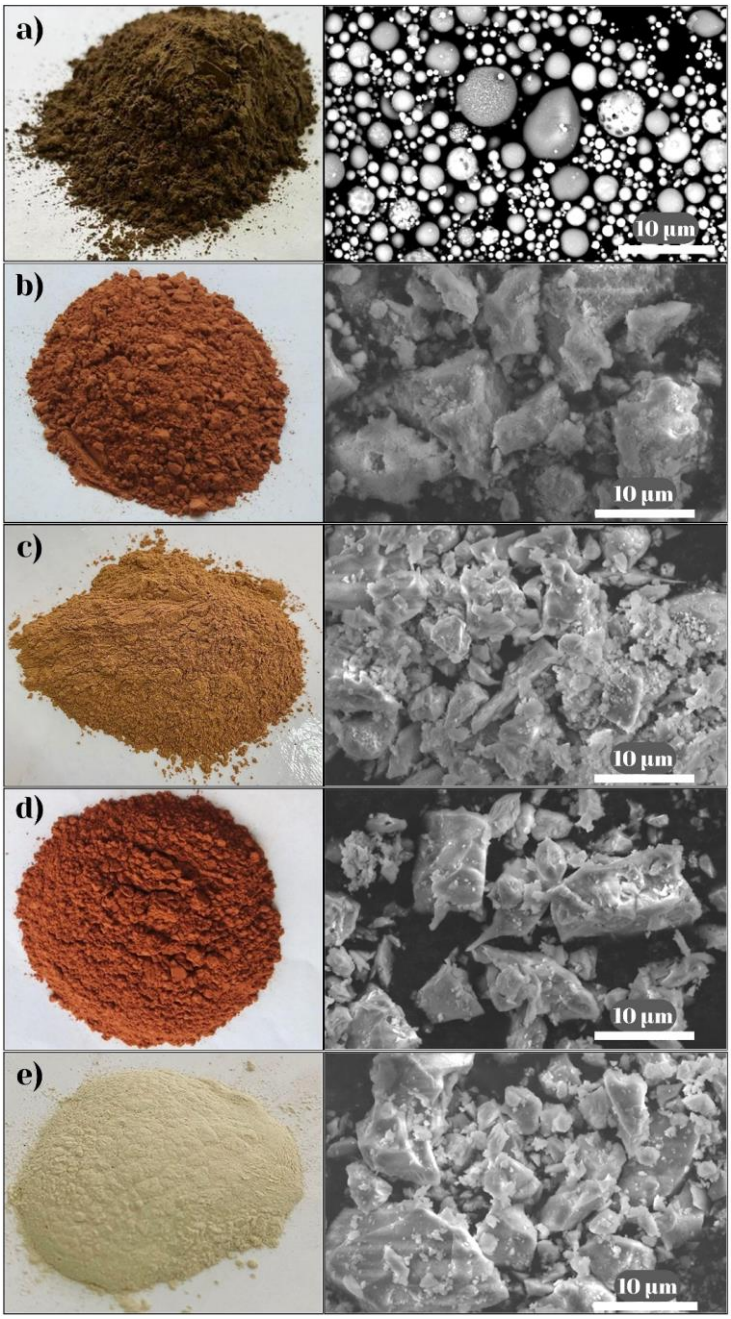

Figure 4. Powder and SEM image of A. fly ash (FA), B. bricks (BR), C. floor tiles (FT), D. roof tiles (RT) and E. sanitary (ST)

2.3. Testing Method

After the mixing process of the fresh geopolymer mixture was completed, ensuring consistency and uniformity, setting time was measured employing the Vicat needle apparatus in accordance with the guidelines provided by SNI 03-6827-2002 [30]. The apparatus consists of a needle, which was steadily lowered into the fresh mixture at regular time intervals until it failed to penetrate the surface. However, as the geopolymer mix demonstrated quick or flash setting, the measurement of the initial setting time was neglected in this experiment. Only the final setting time was then recorded.

A total of three mortar samples were prepared for each mix, and each sample was cast into a cube with sides measuring 50 mm. To assess the strength development over time, compressive strength tests were conducted at dedicated mortar ages 7, 14, and 28 days. The compression testing machine with a capacity of 2000 kN was used for this test, employing a loading rate of 1 kN/s. This testing procedure adhered to ASTM C109 [31].

2.4. Analytical Measurements

The geopolymer remnants from compressive test residue were analyzed in their mineral phase using the random powder method of X-ray diffraction (XRD). The rubble was finely ground, and the analysis was conducted using a PANalytical Xpert 3 XRD device with Cu-Kα as an X-ray source operating at 40 kV and 30 mA. To identify phases

within the geopolymer specimens, HighScore software was employed, complemented by the International Centre for Diffraction Data (ICDD) database.

The finely powdered mortar samples were also prepared for Fourier-transform infrared spectroscopy (FTIR) analysis. The FTIR test was carried out using a Bruker Invenio FTIR spectroscopy instrument, and the spectral data were recorded within the range of 4000–400 cm^{-1}. Subsequently, the obtained spectra were processed and interpreted to identify the chemical components and bonds within the mortar.

Scanning electron microscopy (SEM) analysis was conducted on some of the mortar samples. The selected samples were carefully sliced into a small chip to expose their internal structure. This chip was then mounted using resin and subsequently polished to achieve a smooth and flat surface for analysis. The SEM instrument utilized in this study is the Thermo Scientific™ Quattro SEM, operating at a magnification of 500x, employing the backscattered electron (BSE) method. This approach allows for the detailed examination of the mortar's geopolymer matrix, binder-aggregate bonding, and the presence of particles within the sample.

3. Results and Discussions

3.1. Setting Time

The replacement of fly ash with CWP exhibited a substantial reduction in setting time across all the formulations, as illustrated in Figure 5. In the control sample GC, the setting time measured around 35 minutes, whereas the inclusion of BT and RT showed a profound reduction, with a setting time of only around 18 minutes at 50% inclusion. Moreover, the FT and ST constituents influenced a more subtle decrease in setting time over the replacement levels. This rapid hardening rate of the geopolymer could occur in type C fly ash [32, 33], with respect to the high calcium reaction in an alkaline medium. However, this accelerated setting time could be responsible for the early strength performance. The incorporation of substituted CWP either provides more reactive calcium or absorbs more water during mixing, which appears to facilitate a faster setting process. It was also stated that there was a linear relationship between setting time and flowability, which represented reduced setting time with respect to reduced flowability [34]. These types of mixtures can be considered beneficial, particularly in scenarios where a quick setting time is of importance.

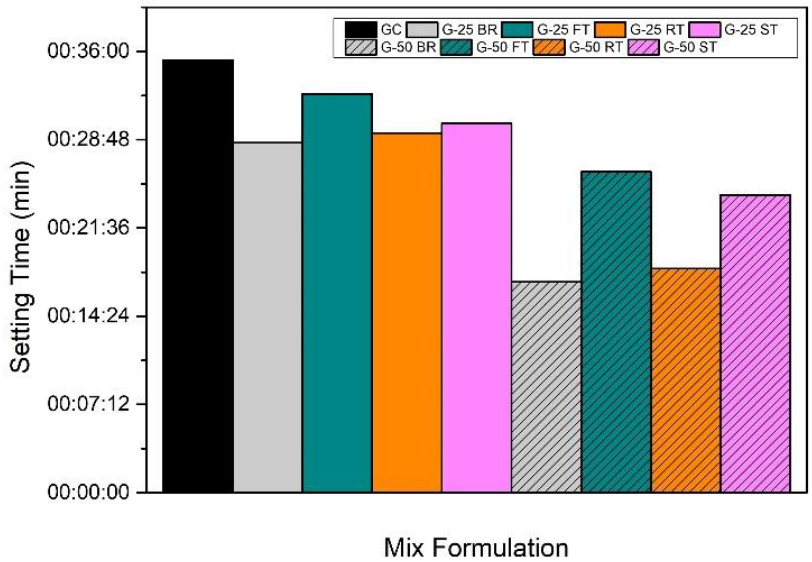

Figure 5. Final setting time of FA-CWP geopolymer

3.2. Compressive Strength

The result of the compressive strength of all specimens at each specified age can be seen in Figure 6. Increasing the percentage of CWP substitution for fly ash as a precursor from 0% to 50% causes a progressive decrease in the compressive strength of the specimens. This was explained that the reduced amount of calcium due to replacement with less reactive materials would result in lower strength, where C-(A)-S-H gel formation is the decisive factor in this process [34]. This phenomenon could also be linked to the faster setting time when applying more replacement, where insufficient reaction time hinder the growing strength of geopolymer. The graph also shows that, in general, the longer the age of the specimen, the compressive strength will increase due to the extended curing time.

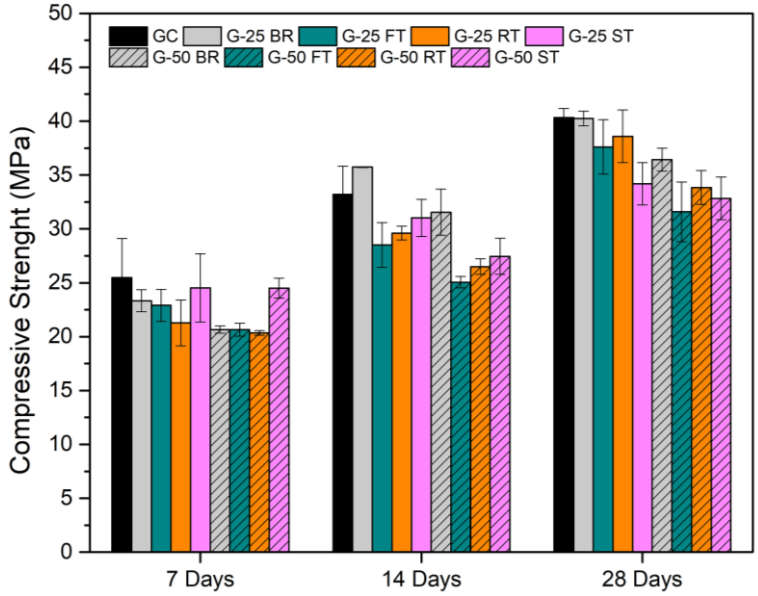

Figure 6. Compressive strength of FA-CWP geopolymer upon respective ages

From the data obtained, bricks were found to be the most promising substitution material when compared to the other constituents, primarily due to their higher compressive strength at 14 and 28 days. This phenomenon could be attributed to the presence of anorthite mineral in BT, which acts as a reactive component in an alkaline medium [35]. This result indicated that brick powder may have the potential to effectively replace fly ash in geopolymer mortar at 25%, especially as the mortar could gain early strength.

On the other hand, the other ceramic constituents demonstrated diminished compressive strength. This may rely on the increased unreacted particles during gel formation. It can also be corroborated with the setting time data, experiencing faster hardening along with more ceramic powder inclusion. The gradual reduction in compressive strength as the effect of ceramic powder was also confirmed with previous studies with respect to each component, ceramic tiles, roof tiles, and sanitary.

3.3. X-ray Diffraction (XRD)

The X-ray diffraction (XRD) diffractogram displayed in Figure 7, displayed a comprehensive view of the crystalline phases detected within various geopolymer samples, encompassing GC, G-50 BR, G-50 FT, G-50 RT, and G-50 ST. The diffraction peaks detected at varied diffraction angles indicate the presence of identical crystalline phases in all these samples. Specifically, the identified phases include calcite ($CaCO_3$), quartz (SiO_2), hematite (Fe_2O_3), mullite ($Al_2O_3 \cdot 2SiO_2$), and plagioclase (anorthite $CaAl_2Si_2O_8$ or albite $NaAlSi_3O_8$). It was also reported by previous research that phases like anorthite [36] and albite [37] emerged in the fly ash-based geopolymer.

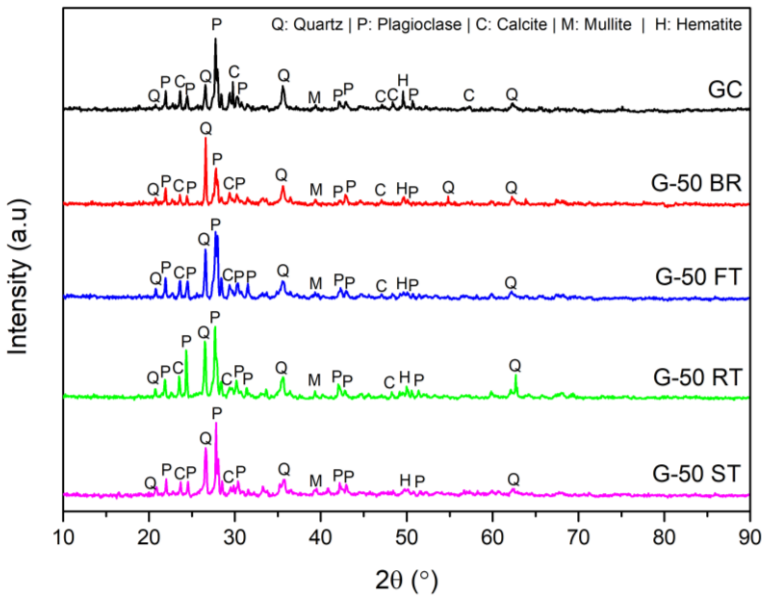

Figure 7. XRD pattern of geopolymer specimen

The presence of the plagioclase phase represented the formation of the geopolymer reaction as this phase was absent in the raw materials, except for BR powder. Again, it was of interest that G-50 BR showed a significant difference in the peak intensity, especially for the quartz and plagioclase. As plagioclase in the form of anorthite was included in the BR, the geopolymer product did not generate increased phase intensity. In contrast, all the other constituents and the GC specimens revealed significant leaps of plagioclase. The intensifying peak of the plagioclase form of albite and anorthite could be attributed to the influence of calcium oxide and Na^+ alkaline reagent [35]. The crystalline anorthite phase could be attributed to the interaction between CaO and the aluminosilicate phase [38]. This can also be ascribed to the reduction of Si in quartz intensity, which then reacts with surrounding molecules of Al and Ca or Na.

The existence of calcite was clearly linked to the nature of high calcium fly ash, which could impact the geopolymer's performance. Similarly, hematite pointed to the inclusion of iron-bearing components, which may influence mechanical characteristics as well. Mullite was associated with the ceramic mineral group, which seemed stable under alkaline conditions. Additionally, with identical results, transitioning from fly ash to CWP may have comparable effect on the formation of the geopolymer matrix without transforming the crystalline and structural properties. This result can be an indication that the studied CWP has significant potential to be used as a substitute for traditional precursors like fly ash in geopolymer synthesis.

3.4. Fourier Transform Infrared Spectroscopy (FTIR)

Figure 8 displays the Fourier-Transform Infrared (FTIR) spectra of various geopolymer samples, including GC, G-50 BR, G-50 FT, G-50 RT, and G-50 ST, which has revealed promising insights into their potential as substitutes for fly ash in the precursor role. The notable similarity in FTIR spectral features among these samples underscores their potential for replacing fly ash in geopolymer synthesis. These FTIR spectra revealed distinct features that provide indications of the chemical composition and bonding characteristics of these geopolymer mixtures. One of the prominent features observed in the FTIR spectra is the presence of broad absorption bands within the approximate range of 3300-3500 cm^{-1}. These bands are attributed to the stretching vibration of O-H bonds, suggesting the presence of hydroxyl groups in the geopolymer samples. The weak peaks around ~1600 cm^{-1} are indicative of the bending vibration of O-H bonds, further confirming the presence of hydroxyl functional groups [39].

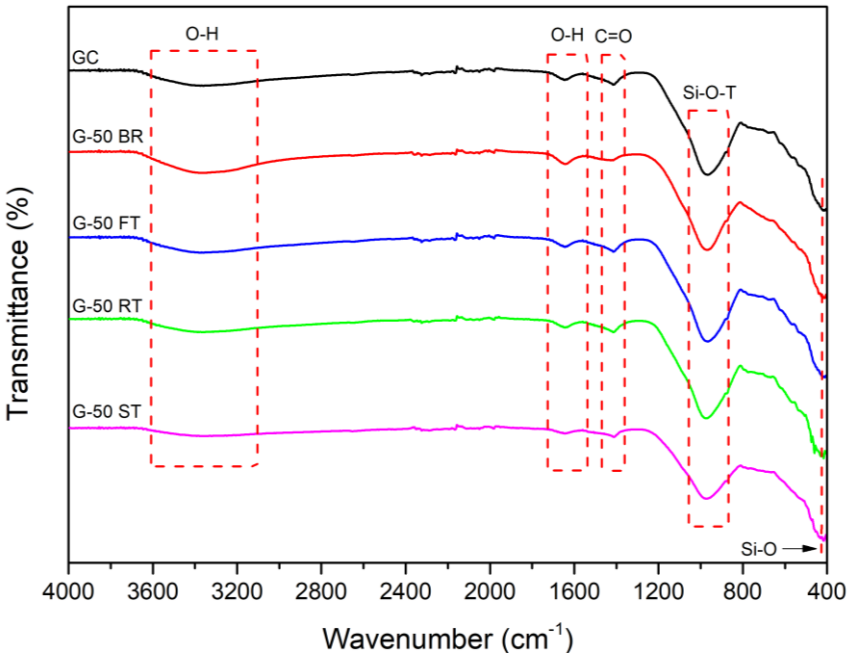

Figure 8. FTIR spectra of geopolymer specimen

In the wavenumber range of 1500-1700 cm^{-1}, distinct peaks corresponding to C=O (carbonyl) bonds are observed. These peaks indicate the presence of carbonyl groups in the geopolymer samples, which can be attributed to the precursors or additives employed in their production. Within the region of 900-1200 cm^{-1}, the FTIR spectra exhibited distinct peaks associated with Si-O-T bonds. The peak observed at around 970 cm^{-1} is attributed to the asymmetric stretching vibration of the Si-O-T (T = Si or Al) bonds [40, 41], in which T represents the tetrahedral bonds. This is a crucial observation as it indicates the presence of silicon and aluminum bonds in the geopolymer matrix. This spectral band can also be attributed to the degree of polysialation and inclusion of aluminum [42], which prominently corresponds to the geopolymer reaction. It is worth noting that all the geopolymer mixtures with the inclusion of ceramic

waste powder showed aluminosilicate polymerization in this area. The reduced intensity seen in G-50ST could indicate a greater incorporation of Al, resulting in a lower Si/Al ratio and thus broadens the frequency. Additionally, a peak at around 400 cm^{-1} was detected, indicating the presence of Si-O bonding [43]. This peak further confirms the presence of silicon bonds in the geopolymer samples, thereby reinforcing the notion that the geopolymerization process has occurred.

3.5. FTIR Spectra of Geopolymer Specimen

The microstructure of geopolymer specimens can be seen in Figure 9. Generally, it is obvious that the connection between the binder and the sand aggregate can be identified. Pores have also been found in the binder system of all mixtures, with ST samples presenting the most pronounced pores. GC microstructures represented weaker bonds between matrix and sand aggregates compared to that of BT and RT inclusion. Furthermore, the binder comprised of geopolymer matrix with the significant presence of unreacted fly ash particles. This was investigated that the presence of calcium could trigger a mechanism involving heterogeneous nucleation and crystallization [44]. The unreacted fly ash particles can be found within the matrix, displaying varying degrees of adherence to the gel [45]. Therefore, the particles have the potential to function as filler material connected with the matrix.

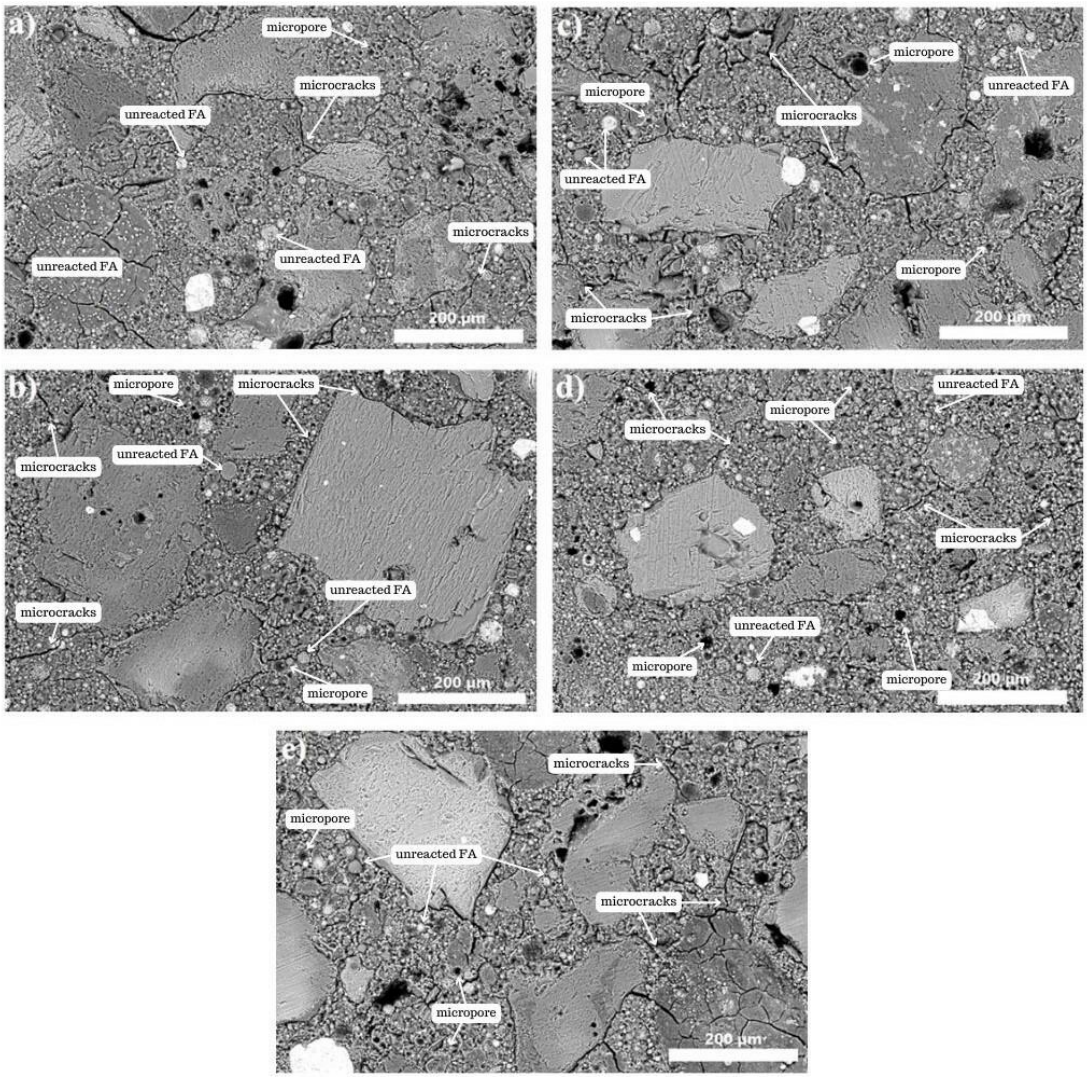

Figure 9. SEM images of geopolymer (a) GC, (b) G-25 BR, (c) G-25 FT, (d) G-25 RT, (e) G-25 ST

The prior rapid solidification characteristic of the fresh geopolymer mixtures could also affect the quantity of these unreacted particles. This may be explained by the insufficient time required for the particles to react with an alkaline solution to form a geopolymer matrix. Therefore, the rate of solidification occurred shortly before the particles completely dissolved, resulting in heterogeneous particles and crystalline phases. It was reported that a high amount of Na_2O in the binder can also lead to the flash setting, which could result in unreacted particulate, voids, and cracks inside the geopolymer matrix [46]. Therefore, it can be seen that fractioning occurred at certain binder-aggregate interfaces and in growing voids in the binder matrix.

4. Conclusion

In conclusion, our experiment revealed several significant findings. Firstly, the addition of brick waste powder (BT) in the geopolymer mortar exhibited comparable results to the control sample, while the incorporation of other types of materials tended to slightly decrease the compressive strength. Moreover, the replacement of BT for the precursor noticeably influenced the setting time of the material, indicating the impact of this substitution on its strength performance. Notably, the compressive strength of samples with 25% BT powder replacement showed superior early strength compared to the control sample at 14 days, though both achieved similar strength levels after 28 days. XRD analysis identified a substantial presence of plagioclase minerals in all samples, likely resulting from alumino-silicate reactions occurring within an alkaline environment. FTIR spectra provided details into specific elemental bonds corresponding to geopolymer reactions, particularly at the peak representing the Si-O-T bond between 900-1200 cm^{-1}. Microstructural evaluation unveiled a geopolymer matrix with some remaining unreacted fly ash particles. The interfacial bond between the matrix and sand aggregates appeared strong in both the GC and G-25 BR, which could be linked to higher strength than other waste ceramic components. Remarkably, all samples exhibited similar frequencies in this range. These findings collectively contribute to our understanding of the effects of various types of ceramic waste powder on the geopolymer properties, offering valuable potential applications in the future. The selection of the type of substitution CWP material and the appropriate substitution ratio remain crucial factors in developing efficient geopolymer mortar.

5. Declarations

5.1. Author Contributions

Conceptualization, E.W.; methodology, B.H.; data curation, B.N., E.D.Y., and J.J.; writing—original draft preparation, I.P. and A.R.; writing—review and editing, B.D.E.; visualization, A.R. and E.D.Y.; supervision, B.H. and S.S.; project administration, S.R.; funding acquisition, S.S. All authors have read and agreed to the published version of the manuscript.

5.2. Data Availability Statement

The data presented in this study are available on request from the corresponding author.

5.3. Funding

This study has been funded by the Research Organization for Nanotechnology and Materials (RP NMM) 13/ III.10.1/HK/2023 No. 26.

5.4. Acknowledgements

The authors express their gratitude to the Research Organization for Nanotechnology and Materials (RP-MM) BRIN for their support, which enabled the successful completion of this research. We extend our thanks to the dedicated laboratories under ELSA BRIN and the Department of Civil Engineering at ITENAS for their invaluable assistance in conducting the analytical and mechanical measurements. Furthermore, thank you to Yudatomo Tri Nugroho from Paiton Power Plant for generously providing fly ash for this study.

5.5. Conflicts of Interest

The authors declare no conflict of interest.

6. References

[1] Mohamad, N., Muthusamy, K., Embong, R., Kusbiantoro, A., & Hashim, M. H. (2022). Environmental impact of cement production and Solutions: A review. Materials Today: Proceedings, 48, 741–746. doi:10.1016/j.matpr.2021.02.212.

[2] Jiang, J., Ye, B., & Liu, J. (2019). Peak of CO2 emissions in various sectors and provinces of China: Recent progress and avenues for further research. Renewable and Sustainable Energy Reviews, 112, 813–833. doi:10.1016/j.rser.2019.06.024.

[3] Spinelli, M., Romano, M. C., Consonni, S., Campanari, S., Marchi, M., & Cinti, G. (2014). Application of Molten Carbonate Fuel Cells in Cement Plants for CO2 Capture and Clean Power Generation. Energy Procedia, 63, 6517–6526. doi:10.1016/j.egypro.2014.11.687.

[4] Singh, R. L., & Singh, P. K. (2017). Global Environmental Problems. Principles and Applications of Environmental Biotechnology for a Sustainable Future. Applied Environmental Science and Engineering for a Sustainable Future. Springer, Singapore. doi:10.1007/978-981-10-1866-4_2.

[5] Taki, K., Mukherjee, S., Patel, A. K., & Kumar, M. (2020). Reappraisal review on geopolymer: A new era of aluminosilicate binder for metal immobilization. Environmental Nanotechnology, Monitoring & Management, 14, 100345. doi:10.1016/j.enmm.2020.100345.

[6] Zhuang, X. Y., Chen, L., Komarneni, S., Zhou, C. H., Tong, D. S., Yang, H. M., Yu, W. H., & Wang, H. (2016). Fly ash-based geopolymer: Clean production, properties and applications. Journal of Cleaner Production, 125, 253–267. doi:10.1016/j.jclepro.2016.03.019.

[7] Amran, M., Debbarma, S., & Ozbakkaloglu, T. (2021). Fly ash-based eco-friendly geopolymer concrete: A critical review of the long-term durability properties. Construction and Building Materials, 270. doi:10.1016/j.conbuildmat.2020.121857.

[8] Hlaváček, P., Šmilauer, V., Škvára, F., Kopecký, L., & Šulc, R. (2015). Inorganic foams made from alkali-activated fly ash: Mechanical, chemical and physical properties. Journal of the European Ceramic Society, 35(2), 703–709. doi:10.1016/j.jeurceramsoc.2014.08.024.

[9] Soutsos, M., Boyle, A. P., Vinai, R., Hadjierakleous, A., & Barnett, S. J. (2016). Factors influencing the compressive strength of fly ash based geopolymers. Construction and Building Materials, 110, 355–368. doi:10.1016/j.conbuildmat.2015.11.045.

[10] Al-Majidi, M. H., Lampropoulos, A., Cundy, A., & Meikle, S. (2016). Development of geopolymer mortar under ambient temperature for in situ applications. Construction and Building Materials, 120, 198–211. doi:10.1016/j.conbuildmat.2016.05.085.

[11] Azevedo, A. R. G., Vieira, C. M. F., Ferreira, W. M., Faria, K. C. P., Pedroti, L. G., & Mendes, B. C. (2020). Potential use of ceramic waste as precursor in the geopolymerization reaction for the production of ceramic roof tiles. Journal of Building Engineering, 29. doi:10.1016/j.jobe.2019.101156.

[12] Hwang, C. L., Damtie Yehualaw, M., Vo, D. H., & Huynh, T. P. (2019). Development of high-strength alkali-activated pastes containing high volumes of waste brick and ceramic powders. Construction and Building Materials, 218, 519–529. doi:10.1016/j.conbuildmat.2019.05.143.

[13] Mahmoodi, O., Siad, H., Lachemi, M., Dadsetan, S., & Sahmaran, M. (2021). Development and characterization of binary recycled ceramic tile and brick wastes-based geopolymers at ambient and high temperatures. Construction and Building Materials, 301. doi:10.1016/j.conbuildmat.2021.124138.

[14] Luhar, I., Luhar, S., Abdullah, M. M. A. B., Nabiałek, M., Sandu, A. V., Szmidla, J., Jurczyńska, A., Razak, R. A., Aziz, I. H. A., Jamil, N. H., & Deraman, L. M. (2021). Assessment of the suitability of ceramic waste in geopolymer composites: An appraisal. Materials, 14(12). doi:10.3390/ma14123279.

[15] Allaoui, D., Nadi, M., Hattani, F., Majdoubi, H., Haddaji, Y., Mansouri, S., Oumam, M., Hannache, H., & Manoun, B. (2022). Eco-friendly geopolymer concrete based on metakaolin and ceramics sanitaryware wastes. Ceramics International, 48(23), 34793–34802. doi:10.1016/j.ceramint.2022.08.068.

[16] Naenudon, S., Wongsa, A., Ekprasert, J., Sata, V., & Chindaprasirt, P. (2023). Enhancing the properties of fly ash-based geopolymer concrete using recycled aggregate from waste ceramic electrical insulator. Journal of Building Engineering, 68. doi:10.1016/j.jobe.2023.106132.

[17] Yanti, E. D., Mubarok, L., Subari, Erlangga, B. D., Widyaningsih, E., Jakah, Pratiwi, I., Rinovian, A., Nugroho, T., & Herbudiman, B. (2024). Utilization of various ceramic waste as fine aggregate replacement into fly ash-based geopolymer. Materials Letters, 357. doi:10.1016/j.matlet.2023.135651.

[18] Kamseu, E., Akono, A. T., Nana, A., Kaze, R. C., & Leonelli, C. (2021). Performance of geopolymer composites made with feldspathic solid solutions: Micromechanics and microstructure. Cement and Concrete Composites, 124. doi:10.1016/j.cemconcomp.2021.104241.

[19] Scanferla, P., Conte, A., Sin, A., Franchin, G., & Colombo, P. (2021). The effect of fillers on the fresh and hardened properties of 3D printed geopolymer lattices. Open Ceramics, 6. doi:10.1016/j.oceram.2021.100134.

[20] Rashad, A. M., Essa, G. M. F., Mosleh, Y. A., & Morsi, W. M. (2023). Valorization of Ceramic Waste Powder for Compressive Strength and Durability of Fly Ash Geopolymer Cement. Arabian Journal for Science and Engineering, 1-13. doi:10.1007/s13369-023-08428-x.

[21] Bhavsar, J. K., & Panchal, V. (2022). Ceramic Waste Powder as a Partial Substitute of Fly Ash for Geopolymer Concrete Cured at Ambient Temperature. Civil Engineering Journal (Iran), 8(7), 1369–1387. doi:10.28991/CEJ-2022-08-07-05.

[22] Sarkar, M., & Dana, K. (2021). Partial replacement of metakaolin with red ceramic waste in geopolymer. Ceramics International, 47(3), 3473–3483. doi:10.1016/j.ceramint.2020.09.191.

[23] Bayer Öztürk, Z., & Atabey, İ. İ. (2022). Mechanical and microstructural characteristics of geopolymer mortars at high temperatures produced with ceramic sanitaryware waste. Ceramics International, 48(9), 12932–12944. doi:10.1016/j.ceramint.2022.01.166.

[24] Hajimohammadi, A., & van Deventer, J. S. J. (2016). Dissolution behaviour of source materials for synthesis of geopolymer binders: A kinetic approach. International Journal of Mineral Processing, 153, 80–86. doi:10.1016/j.minpro.2016.05.014.

[25] Ranjbar, N., Kuenzel, C., Spangenberg, J., & Mehrali, M. (2020). Hardening evolution of geopolymers from setting to equilibrium: A review. Cement and Concrete Composites, 114. doi:10.1016/j.cemconcomp.2020.103729.

[26] Li, Z., Gao, Y., Zhang, J., Zhang, C., Chen, J., & Liu, C. (2021). Effect of particle size and thermal activation on the coal gangue based geopolymer. Materials Chemistry and Physics, 267. doi:10.1016/j.matchemphys.2021.124657.

[27] Zhang, J., Li, S., Li, Z., Liu, C., & Gao, Y. (2020). Feasibility study of red mud for geopolymer preparation: effect of particle size fraction. Journal of Material Cycles and Waste Management, 22(5), 1328–1338. doi:10.1007/s10163-020-01023-4.

[28] Assi, L. N., Eddie Deaver, E., & Ziehl, P. (2018). Effect of source and particle size distribution on the mechanical and microstructural properties of fly Ash-Based geopolymer concrete. Construction and Building Materials, 167, 372–380. doi:10.1016/j.conbuildmat.2018.01.193.

[29] ASTM C618-12a. (2017). Coal Fly Ash and Raw or Calcined Natural Pozzolan for Use in Concrete. ASTM International, Pennsylvania, United States. doi:10.1520/C0618-12.

[30] SNI 03-6827-2002. (2002). Standard Test Method for Setting Time of Hydraulic Cement for Civil Engineering. National Standardization Agency of Indonesia, Jakarta, Indonesia.

[31] ASTM C109/C109M-20b. (2021). Standard Test Method for Compressive Strength of Hydraulic Cement Mortars. ASTM International, Pennsylvania, United States. doi:10.1520/C0109_C0109M-20B.

[32] Topark-Ngarm, P., Chindaprasirt, P., & Sata, V. (2015). Setting Time, Strength, and Bond of High-Calcium Fly Ash Geopolymer Concrete. Journal of Materials in Civil Engineering, 27(7), 04014198. doi:10.1061/(asce)mt.1943-5533.0001157.

[33] Leonard Wijaya, A., Jaya Ekaputri, J., & Triwulan. (2017). Factors influencing strength and setting time of fly ash based-geopolymer paste. MATEC Web of Conferences, 138. doi:10.1051/matecconf/201713801010.

[34] Huseien, G. F., Sam, A. R. M., Shah, K. W., Asaad, M. A., Tahir, M. M., & Mirza, J. (2019). Properties of ceramic tile waste based alkali-activated mortars incorporating GBFS and fly ash. Construction and Building Materials, 214, 355–368. doi:10.1016/j.conbuildmat.2019.04.154.

[35] González-García, D. M., Téllez-Jurado, L., Jiménez-Álvarez, F. J., & Balmori-Ramírez, H. (2017). Structural study of geopolymers obtained from alkali-activated natural pozzolan feldspars. Ceramics International, 43(2), 2606–2613. doi:10.1016/j.ceramint.2016.11.070.

[36] Nergis, D. D. B., Abdullah, M. M. A. B., Sandu, A. V., & Vizureanu, P. (2020). XRD and TG-DTA study of new alkali activated materials based on fly ash with sand and glass powder. Materials, 13(2), 343. doi:10.3390/ma13020343.

[37] Amin, M., Sudibyo, S., Birawidha, D. C., Rinovian, A., Erlangga, B. D., Al Muttaqqi, M., Suka, E. G., & Pratiwi, S. (2023). Effect of bentonite on fly ash and bottom ash based engineered geopolymer composite. Riset Geologi Dan Pertambangan, 33(1), 1225. doi:10.55981/risetgeotam.2023.1225.

[38] Derouiche, R., Zribi, M., & Baklouti, S. (2023). Study of Carbonated Clay-Based Phosphate Geopolymer: Effect of Calcite and Calcination Temperature. Minerals, 13(2), 284. doi:10.3390/min13020284.

[39] Azimi, E. A., Abdullah, M. M. A. B., Vizureanu, P., Salleh, M. A. A. M., Sandu, A. V., Chaiprapa, J., Yoriya, S., Hussin, K., & Aziz, I. H. (2020). Strength development and elemental distribution of dolomite/fly ash geopolymer composite under elevated temperature. Materials, 13(4), 1015. doi:10.3390/ma13041015.

[40] Rees, C. A., Provis, J. L., Lukey, G. C., & Van Deventer, J. S. J. (2007). In situ ATR-FTIR study of the early stages of fly ash geopolymer gel formation. Langmuir, 23(17), 9076–9082. doi:10.1021/la701185g.

[41] Yusuf, M. O. (2023). Bond Characterization in Cementitious Material Binders Using Fourier-Transform Infrared Spectroscopy. Applied Sciences (Switzerland), 13(5), 3353. doi:10.3390/app13053353.

[42] Zaharaki, D., Komnitsas, K., & Perdikatsis, V. (2010). Use of analytical techniques for identification of inorganic polymer gel composition. Journal of Materials Science, 45(10), 2715–2724. doi:10.1007/s10853-010-4257-2.

[43] Toniolo, N., Taveri, G., Hurle, K., Roether, J. A., Ercole, P., Dlouhý, I., & Boccaccini, A. R. (2017). Fly-ash-based geopolymers: How the addition of recycled glass or red mud waste influences the structural and mechanical properties. Journal of Ceramic Science and Technology, 8(3), 411–419. doi:10.4416/JCST2017-00053.

[44] Temuujin, J., van Riessen, A., & Williams, R. (2009). Influence of calcium compounds on the mechanical properties of fly ash geopolymer pastes. Journal of Hazardous Materials, 167(1–3), 82–88. doi:10.1016/j.jhazmat.2008.12.121.

[45] Lloyd, R. R., Provis, J. L., & Van Deventer, J. S. J. (2009). Microscopy and microanalysis of inorganic polymer cements. 2: The gel binder. Journal of Materials Science, 44(2), 620–631. doi:10.1007/s10853-008-3078-z.

[46] Feng, M., Jiang, C., Wang, Y., Zou, Y., & Zhao, J. (2023). Experimental Study on Mechanical Properties and Drying Shrinkage Compensation of Solidified Ultra-Fine Dredged Sand Blocks Made with GGBS-Based Geopolymer. Buildings, 13(7), 1750. doi:10.3390/buildings13071750.